ORIGINAL ARTICLES

LOCAL SCATTERING ANISOTROPY OF THE SKIN AS A POSSIBLE FACTOR OF FLUORESCENCE BORDERS DISTORTION OF NEOPLASMS

Kiryushchenkova N.P.[1], **Novikov I.A.**[1,2]
[1]M.M. Krasnov Research Institute of Eye Diseases, Moscow, Russia
[2]Prokhorov General Physics Institute of Russian Academy of Sciences, Moscow, Russia

Abstract

The use of protoporphyrin IX fluorescence imaging in skin tumors is limited by the complexity of light propagation in tissues. A non-invasive scattering anisotropy test (comparison of the fluorescence pattern of a tumor with that of a point source applied to the same spot) would be useful in distinguishing between cases of subsurface tumor growth and local fluorescence pattern distortions. However, the knowledge is missing of whether the distribution from an external light source would be representative. The experiment described here addressed the correlation between patterns in which light is dispersed from an external and an internal source within the same area of the skin. A pig's head was chosen as the model. Four zones of interest were identified, all different in optical properties. The wavelength of the light source was selected as to simulate the PpIX fluorescence. The correspondence of light distribution patterns was quantified using the correlation method. The results have clearly demonstrated the strong relationship between the fluorescence distribution pattern of a tumor and the condition/topography of the surrounding tissues and proved the possibility of using an external light source to assess the local scattering anisotropy of the skin *in vivo*.

Keywords: scattering anisotropy, skin neoplasm, fluorescence, tumor border, protoporphyrin IX.

Contacts: Nataliya Kiryushchenkova, e-mail: nkir@niigb.ru

For citations: Kiryushchenkova N.P., Novikov I.A. Local scattering anisotropy of the skin as a possible factor of fluorescence borders distortion of neoplasms, *Biomedical Photonics*, 2025, vol. 14, no. 2, pp. 12–20. doi: 10.24931/2413–9432–2025–14–2–12–20

ЛОКАЛЬНАЯ АНИЗОТРОПИЯ РАССЕЯНИЯ КОЖИ КАК ВОЗМОЖНЫЙ ФАКТОР ИСКАЖЕНИЯ ФЛУОРЕСЦЕНТНЫХ ГРАНИЦ ОПУХОЛИ

Н.П. Кирющенкова[1], **И.А. Новиков**[1,2]
[1]Научно-исследовательский институт глазных болезней им. М.М. Краснова, Москва, Россия
[2]Институт общей физики им. А.М. Прохорова Российской академии наук, Москва, Россия

Резюме

Широкое применение диагностики новообразований кожи на основе анализа флуоресценции протопорфирина IX ограничено сложностью распространения, в частности рассеяния, света в тканях. Для оценки влияния локальной анизотропии рассеяния кожи на картину флуоресценции опухоли предлагается производить сравнение последней с флуоресцентной картиной распространения света от точечного источника, приложенного к поверхности кожи в проекции опухоли. Такой тест был бы полезен для выявления случаев скрытого роста новообразования, однако, репрезентативность его неизвестна. В описанном здесь эксперименте изучалась корреляция между паттернами рассеяния света от внешнего и внутреннего источника в пределах одного и того же участка кожи. Моделью служила голова свиньи. Четыре зоны интереса с различными оптическими свойствами были подобраны с учетом строения средней трети лица человека. Длина волны источника света была выбрана так, чтобы имитировать флуоресценцию протопорфирина IX. Соответствие моделей распределения света было определено количественно корреляционным методом. Полученные результаты наглядно продемонстрировали сильную взаимосвязь между характером распределения флуоресценции опухоли и состоянием/топографией окружающих тканей и доказали возможность использования внешнего источника света для оценки локальной анизотропии рассеяния кожи *in vivo*.

Ключевые слова: анизотропия рассеяния, новообразование кожи, флуоресценция, граница опухоли, протопорфирин IX.

Контакты: Кирющенкова Н.П., nkir@niigb.ru

Для цитирования: Кирющенкова Н.П., Новиков И.А. Локальная анизотропия рассеяния кожи как возможный фактор искажения флуоресцентных границ опухоли // Biomedical Photonics. – 2025. – Т. 14, № 2. – С. 12–20. doi: 10.24931/2413–9432–2025–14–2–12–20

Introduction

Malignant skin neoplasms, well-known for their high incidence worldwide, mainly include basal cell carcinoma (BCC) and other tumors of epithelial origin [1,2]. Close attention is paid to accurately defining tumor borders and optimal surgical margins due to the frequent head and neck localization of BCC and associated complicacy of its removal [3,4].

Biomedical fluorescence imaging, or fluorescence diagnostics, is a compact area of research aimed at assessing tissue concentrations of pathology markers by exciting their characteristic emission. In oncology, one such marker is protoporphyrin IX (PpIX), a precursor of heme, which is known to accumulate in rapidly dividing cells [5-12]. PpIX fluorescence imaging allows detection of increased proliferative activity of the tissue and potentially can help identify areas of subsurface tumor growth [13-15]. Most of the existing techniques of endogenous PpIX fluorescence analysis involve the use of fluorescence induction [13,14], but some authors prefer to work with non-induced endogenous signals [15]. Regardless, the final result of fluorescence imaging greatly depends on skin properties such as the preferential orientation of collagen fibres in the dermis [16-23]. The complexity of light propagation in the skin constrains the development of fluorescence imaging as a diagnostic modality.

We believe that the impact of scattering anisotropy of the skin could be addressed by comparing the actual fluorescence distribution pattern of a tumor with that of a point source emitting at same wavelengths within the same location. In an abstract isotropic model, radiation from a point source would be evenly distributed in all directions and brightness isolines would have the shape of a circle in any section. In reality, however, skin projection of a point light source would not match its original geometry due to scattering anisotropy of the medium. All the distortions thus determined, could then be used to interpret the fluorescence diagnostics results.

Given the absolute impossibility of introducing a point light source directly into a tumor in vivo, we propose that the source may be externally applied to the skin surface. We assume that the light propagation from an internal and an external source will have a high degree of agreement in our case, and thus, the surface source will serve as an acceptable model of intradermal neoplasm fluorescence.

The aim of this study was to prove our assumption and to determine experimentally the correlation between patterns in which light is dispersed from an external and an internal source within the same area of the skin.

Material and methods

A pig's head (collected at a meat processing plant 12 hours after death) was chosen as the model. The head was divided in two parts along the sagittal suture, the brain was removed.

Optical scheme

Light source: we used a 560-660 nm incoherent light source with adjustable intensity built on the basis of the BioSpecLSH-4 (Russia) compact halogen source with a dichroic filter for the simulation of PpIX fluorescence. The source was connected to a 400 μm single-mode optical fiber equipped with a custom made matte hemisphere (diffuser) at its distal end. To deliver the fiber across bones and soft tissues, a Tro-Venocath 16-gauge intravenous cannula (Vogt Medical, Germany) was used.

To study the intensity distribution of light scattered by the diffuser relative to the longitudinal axis of the fiber, we performed the following.

The cannula with the fiber inside was mounted on a bracket able to rotate in the horizontal plane. The axis of rotation was perpendicular to the cannula and passed through the center of the diffuser. A Lesa-01-BioSpec spectrometer (Russia) was installed in the plane of rotation of the cannula. The distance between the aperture of the spectrometer and the diffuser was 10 centimeters. The position of the cannula's axis that coincided with the direction of the spectrometer was taken as 0 degrees.

Light intensity was then evaluated through the *area under curve* (AUC) values of the emission spectrum at various positions of the cannula with respect to the spectrometer. The maximum intensity was obtained at 30 degrees and taken as 1. Other intensities were calculated relatively to this position (Table 1).

Таблица 1
Относительные значения площади под кривой (AUC) спектра излучения при различных положениях источника света относительно спектрометра

Table 1
Relative AUC values of the emission spectrum at various positions of the light source with respect to the spectrometer

Направление, ° Direction, °	0	30	60	90	-90
Относительная интенсивность излучения Relative light intensity	0.79	1.00	0.92	0.94	0.88

Registration system

Digital camera: Canon EOS 2000D (Japan).

Shooting mode: aperture priority, f/8 aperture, 0.6 sec shutter speed, ISO-400, neutral white balance.

Lens distortions were preliminarily evaluated while using a rectangular mesh target.

The camera was mounted on a tripod and fixed in front of the experimental tissue block.

To navigate across the surface of the skin, a LED backlight with a built-in ZS11 filter (480-570 nm) (OLTECH Photonics, Russia) was used.

The wavelength of the backlight was chosen so that it would not interfere with the main signal in the RGB color model. The intensity of the backlight, as well as that of the test source, was within the dynamic range of the camera.

The course of the experiment:

We have planned to study four skin zones with potentially different optical features:

1) a relatively smooth area of skin within one face region,
2) a relatively smooth area of skin at the border between two regions,
3) an area of skin with a pronounced microrelief,
4) an area of skin in the projection of ligaments and/or tendons.

As a result, in step 1, four areas were selected (Fig. 1), including one within the frontal region (zone of interest 1), two in the periorbital region – close to the medial and latheral canthi (zones of interest 2 and 4), and one within the region that corresponds to the nasolacrimal sulcus in humans (zone of interest 3).

Within each of the zones, a 1.8-mm drill was used to create an access to the subcutaneous space from the cranial cavity (Fig. 2A). A skin-mountable strain sensor (GML624A, Galoce, China) was used for depth monitoring (Fig. 2B). During the formation of the bone tunnel, the readings on the sensor fluctuated within the range of +/-0.1 gram-force (gf), which we considered to be mechanical noise. At the value of 0.2 gf, the drilling was stopped. The position of the tip of the drill was then detected using a conical magnetic pendulum and marked on the preliminary photo (Fig. 2C). After this, the drill was removed (Fig. 2D).

In step 2, the light distribution pattern from an internally (intradermally) located light source was recorded (Test 1). For that, an intravenous cannula with the fiber inside was inserted from the cranial cavity into each of the four access tunnels such that the end of the fiber was gently pressed against the dermis (Fig. 2E,F).

In step 3, the light distribution pattern from an externally located light source was recorded (Test 2). For that, the optic fiber was applied to the four spots on the skin surface earlier determined with the pendulum (see step 1) (Fig. 2G,H).

Рис. 1. Расположение зон интереса на модели. Масштаб прямоугольников 1-4 соответствует полученным кадрам.
Fig. 1. Location of the four zones of interest. The scale of the yellow rectangles corresponds to the resultant images.

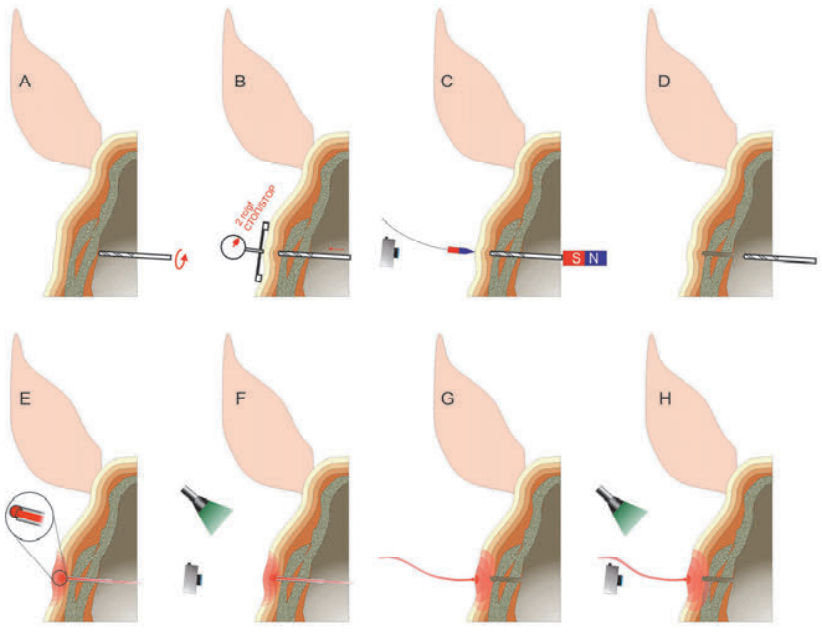

Рис. 2. Последовательность проведения эксперимента. A – сверление доступа со стороны полости черепа; B – остановка сверления; C – определение проекции сверла на поверхность кожи; D – извлечение сверла из сформированного доступа; E – введение интравенозной канюли с помещенным внутрь волноводом; матовая полусфера на конце волокна (врезка); F – фотофиксация картины распределения сигнала от внутрикожного источника (тест 1); G – аппликация волновода на поверхность кожи; H – фотофиксация картины распределения сигнала от наружного источника (тест 2).
Fig. 2. Course of the experiment. A – access drilling from the cranial cavity; B – drilling stop; C – the detection of the tip of the drill projection to the skin; D – drill removal from the created access tunnel; E – introduction of an intravenous cannula with the optical fiber; close view of the fiber end equipped with a matted hemisphere (inset); F – taking photo of the light distribution pattern from an intradermally located light source (Test 1); G – optical fiber application to the skin surface; H – taking photo of the light distribution pattern from a superficially located light source (Test 2).

Image preprocessing

Image preprocessing was done with the ImageJ 1.50d free software (Wayne Rasband National Institutes of Health, USA). Each of the obtained images (Fig. 3A,B) was split into RGB channels. The red channel was then smoothed with a 20-pixel Gaussian window (which exceeds the size of most microstructural elements of the skin, such as hair follicle openings) and posterized (Fig. 3C,D), which made it possible to create isolines of the red channel brightness gradient. After that, the red channel images with traced isolines were combined in pairs in accordance with the four zones of interest such that the first image in each pair was the one obtained at Test 1 (internal light source), and the second – the one obtained at Test 2 (external light source).

Quantitative assessment of the correspondence between skin projections of light distribution at different positions of the source

The skin projection of the tip of the drill determined using a magnetic pendulum (step 1, Fig. 2C) was taken as the origin (0,0). Then, in each pair of images (i.e. Test 1 and Test 2 images of the same zone of interest), brightness isolines were identified being similarly distant from the origin. After that, the distance from the origin to the selected isolines was measured in 24 directions at 15-degree intervals (Fig. 3E). In all cases, the value obtained from the Test 1 isoline was taken as the X-coordinate, while that from the Test 2 isoline – as the Y-coordinate of the same point on the scatter plot. Thus, for each pair of isolines a 24-point X,Y cloud was produced. For each cloud, the *k* coefficient of the linear trend of approximation was calculated.

Estimation of the parameters of ellipses that approximate the isolines of the brightness gradient

For each isoline that was analyzed at the previous stage, the axis ratio of the approximating ellipse was additionally determined with the ImageJ 1.50d free software (Wayne Rasband National Institutes of Health, USA).

Results

The pairs of Test 1 and Test 2 photos (Fig. 4) show the similarity in the overall pattern of light propagation in the skin, regardless of whether the light source was applied externally or located intradermally. Note that the use of the selected smoothing radius resulted in complex-shaped isolines in the second zone of interest, where multiple large pores were present (Fig. 4D-F). Also, in the images taken at the external position of the light source (Fig. 4C,F,I,L), the shape of the isolines was affected to varying degrees by the presence of the fiber in the field of view of the camera.

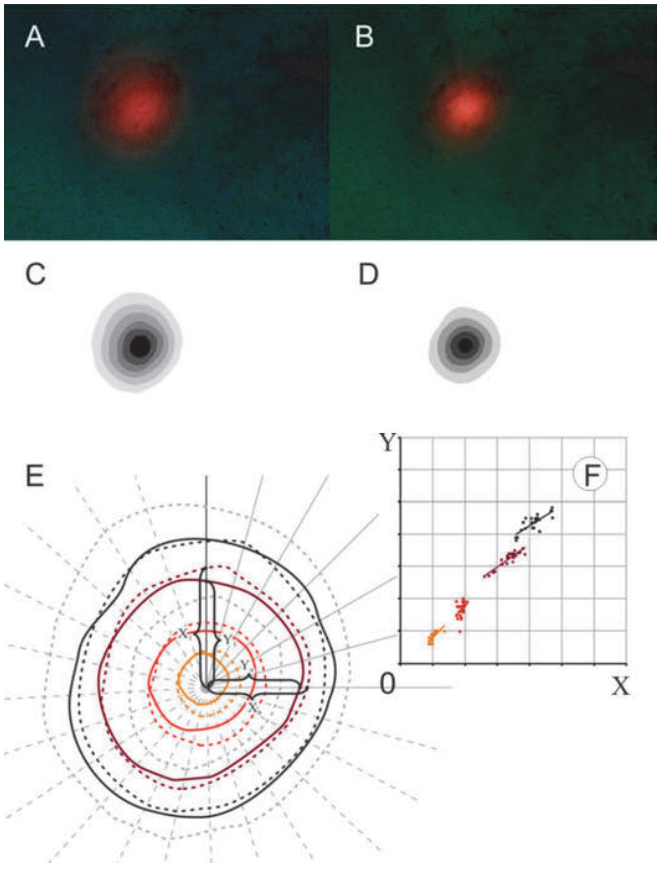

Рис. 3. Порядок обработки изображений (зона интереса 4 в качестве примера). A, B – фотографии одного и того участка кожи, подсвеченных сине-зеленым прожектором, при различном положении источника, имитирующего флуоресценцию протопорфирина IX – внутрикожно (A) или поверхностно (B); C,D – красный канал изображений A,B, соответственно. Применено сглаживание гауссовым окном и постеризация; E – трассированные изолинии градиента яркости красного канала для рисунок C и D, совмещенные по центру координат (пояснение в тексте). Сплошным цветом нанесены изолинии с первого изображения из пары (внутрикожная установка источника, тест 1), пунктиром – со второго (наружная установка источника, тест 2). Показан принцип получения координат X,Y для пары изолиний на сходном удалении от центра. Во всех случаях значение Xn присваивали точке, полученной в тесте 1, Yn – в тесте 2; F – пример диаграммы распределения совокупности точек, полученных для одной зоны интереса.

Fig. 3. Image preprocessing and quantitative assessment example (zone of interest 4). A, B – internal (A) and external (B) position of the PpIX-simulating light source within the same skin area (blue-green backlit). C,D – red channel images derived from A and B photographs, respectively. Gaussian smoothing and posterization are applied. E – traced isolines of the brightness gradient from C and D images, aligned by the origin (explanation in the text). The isolines from the first image of the pair (internal light source) are solid, from the second (external light source) are dotted. The principle of obtaining X- and Y-coordinates from a pair of isolines is shown. In all cases, the Test 1 isoline measurement was taken as the X-coordinate and the Test 2 isoline measurement – as the Y-coordinate of the same point on the scatter plot. F – a scatter plot example, where four X,Y point clouds describe four pairs of isolines chosen for analysis. The measurements were done in 24 directions.

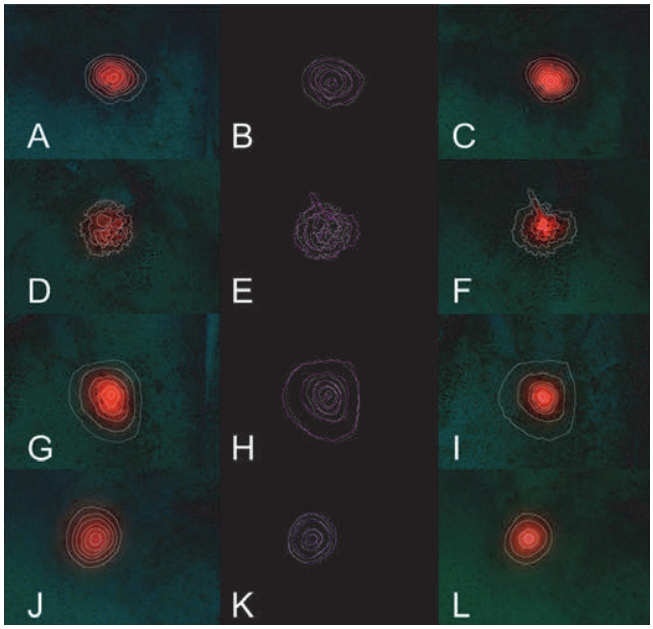

Рис. 4. Оптический результат эксперимента.
Пары фотографий участков кожи (см. зоны интереса на рисунке 1), подсвеченных сине-зеленым прожектором, при различном положении источника, имитирующего флуоресценцию протопорфирина IX – внутрикожно (A, D, G, J) или поверхностно (C, F, I, L). Белым цветом на все фотографии нанесены изолинии градиентов яркости красного канала, которые, кроме того, совмещены по центру координат для каждой пары фотографии и вынесены на отдельное изображение (B, E, H, K). Зоне интереса 1 соответствуют изображения A,B,C; зоне интереса 2 соответствуют изображения D, E, F; зоне интереса 3 – G, H, I; зоне интереса 4 – J, K, L.
Fig. 4. Results of the optical experiment.
Pairs of photographs of the same skin areas (see zones of interest in Fig. 1) at internal (A, D, G, J) and external (C, F, I, L) position of the PpIX-simulating light source (blue-green backlit) with isolines of the red channel brightness gradient applied in white. Additionally, the isolines of the red channel brightness gradient from the corresponding photos are aligned by the origin and presented separately in images B, E, H, K. Images A, B, C correspond to the zone of interest 1; images D, E, F correspond to the zone of interest 2; G, H, I – to the zone of interest 3; J, K, L – to the zone of interest 4.

To assess the correspondence between skin projections of light distribution from an external and an internal source, the scatter diagrams were created for all zones of interest (Fig. 5) such that every X,Y point cloud corresponded to a certain pair of isolines derived from the Test 1 and Test 2 photographs. For quantitative description, the *k* coefficient of the linear trend equation was calculated for each point cloud (Fig. 5, Table 2). As one can see, the correspondence of light distribution increases ($k \to 1$) with distance from the origin in all zones of interest.

The axis ratios of the ellipses approximating the analyzed isolines are also provided in Table 2.

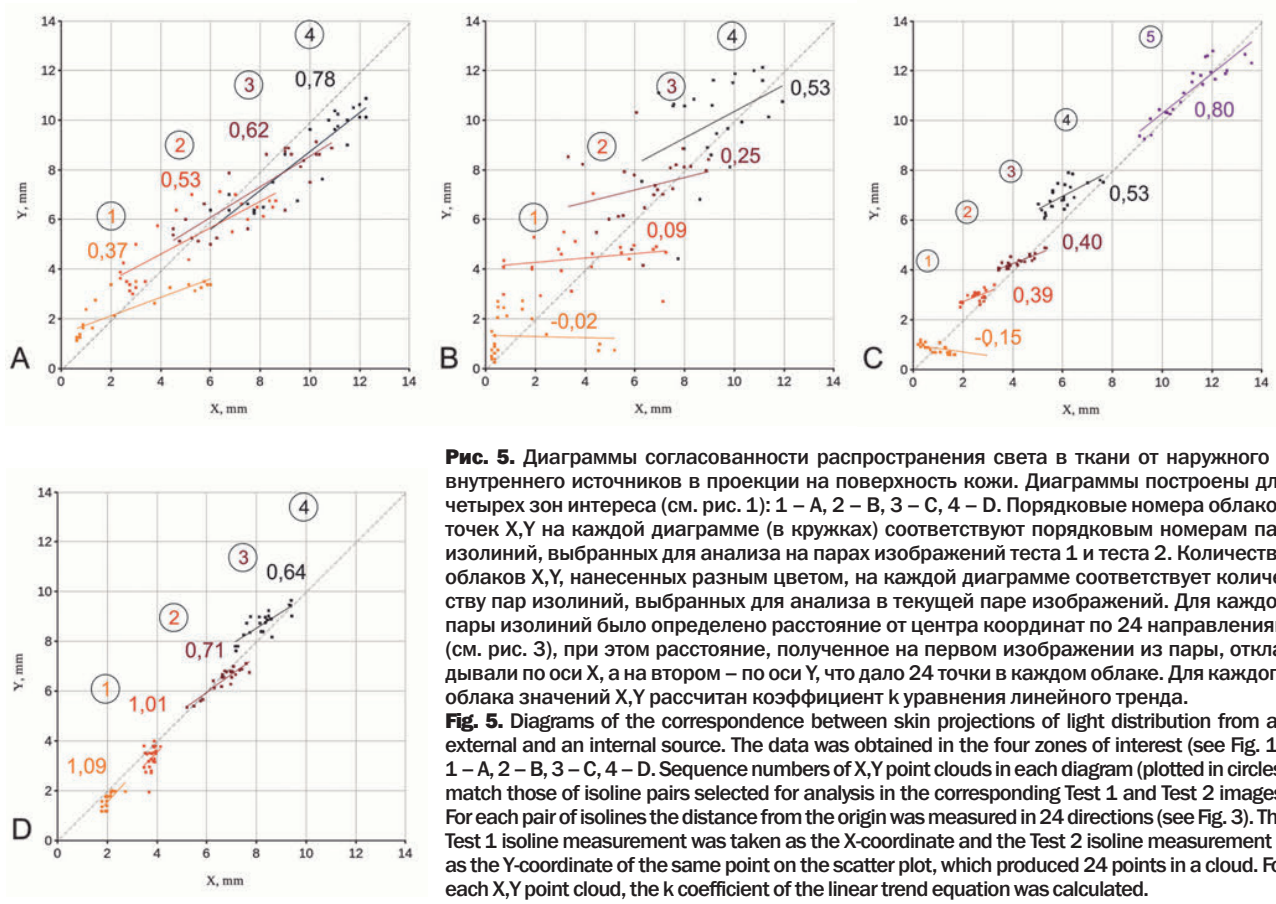

Рис. 5. Диаграммы согласованности распространения света в ткани от наружного и внутреннего источников в проекции на поверхность кожи. Диаграммы построены для четырех зон интереса (см. рис. 1): 1 – A, 2 – B, 3 – C, 4 – D. Порядковые номера облаков точек X,Y на каждой диаграмме (в кружках) соответствуют порядковым номерам пар изолиний, выбранных для анализа на парах изображений теста 1 и теста 2. Количество облаков X,Y, нанесенных разным цветом, на каждой диаграмме соответствует количеству пар изолиний, выбранных для анализа в текущей паре изображений. Для каждой пары изолиний было определено расстояние от центра координат по 24 направлениям (см. рис. 3), при этом расстояние, полученное на первом изображении из пары, откладывали по оси X, а на втором – по оси Y, что дало 24 точки в каждом облаке. Для каждого облака значений X,Y рассчитан коэффициент k уравнения линейного тренда.
Fig. 5. Diagrams of the correspondence between skin projections of light distribution from an external and an internal source. The data was obtained in the four zones of interest (see Fig. 1): 1 – A, 2 – B, 3 – C, 4 – D. Sequence numbers of X,Y point clouds in each diagram (plotted in circles) match those of isoline pairs selected for analysis in the corresponding Test 1 and Test 2 images. For each pair of isolines the distance from the origin was measured in 24 directions (see Fig. 3). The Test 1 isoline measurement was taken as the X-coordinate and the Test 2 isoline measurement – as the Y-coordinate of the same point on the scatter plot, which produced 24 points in a cloud. For each X,Y point cloud, the k coefficient of the linear trend equation was calculated.

Таблица 2
Оценка параметров эллипсов, аппроксимирующих изолинии градиентов яркости*

Table 2
Parameters of ellipses approximating the isolines of the brightness gradient*

	Отношение сторон эллипса (внутренний источник) Axis ratio of the ellipse (internal light source)	Отношение сторон эллипса (наружный источник) Axis ratio of the ellipse (external light source)	Коэффициент уравнения линейного тренда, k Coefficient of the linear trend equation, k
Зона интереса 1 / Zone of interest 1			
Пара изолиний / isoline pair 1	1.37	1.09	0.37
Пара изолиний / isoline pair 2	1.29	1.24	0.53
Пара изолиний / isoline pair 3	1.45	1.30	0.62
Пара изолиний / isoline pair 4	1.48	1.33	0.78
Зона интереса 2 / Zone of interest 2			
Пара изолиний / isoline pair 1	2.73	2.98	-0.02
Пара изолиний / isoline pair 2	1.30	1.11	0.09
Пара изолиний / isoline pair 3	1.01	1.18	0.25
Пара изолиний / isoline pair 4	1.04	1.35	0.53
Зона интереса 3 / Zone of interest 3			
Пара изолиний / isoline pair 1	1.28	1.27	-0.15
Пара изолиний / isoline pair 2	1.84	1.66	0.39
Пара изолиний / isoline pair 3	1.23	1.19	0.40
Пара изолиний / isoline pair 4	1.09	1.10	0.53
Пара изолиний / isoline pair 5	1.27	1.27	0.80
Зона интереса 4 / Zone of interest 4			
Пара изолиний / isoline pair 1	1.04	1.05	1.09
Пара изолиний / isoline pair 2	1.06	1.17	1.01
Пара изолиний / isoline pair 3	1.13	1.13	0.71
Пара изолиний / isoline pair 4	1.20	1.04	0.64

* Пары изолиний пронумерованы от центра координат.
* Pairs of isolines are numerated from the origin.

Discussion

First of all, it should be noted that all designs in this work are practical and do not aim to provide a thorough analysis of quantum light-molecules interactions in the skin.

From an optical point of view, a skin neoplasm can be considered as a complex multicomponent object [16-22]. In the epidermis, a significant portion of the radiation in the range of 350-1200 nm is absorbed by melanin, and in the ultraviolet region (with wavelengths less than 300 nm) the light is absorbed by aromatic amino acids, nucleic acids, urocanoic acid, and other molecules. In the dermis, red blood cell hemoglobin serves as the primary light absorber. Light scattering occurs as well due to the differences in the refractive indices of skin structures. Spatial distribution of scattered light and its intensity depends on the size and shape of these "inhomogeneities" in the medium relative to the wavelength, which, in turn, affects the results of spectral measurements due to the Rayleigh and Mie scattering. Research also shows that these parameters can change over the course of a lifetime due to changes in melanin concentration and collagen density [23].

A significant contribution to the formation of the optical spectrum of the skin is made by endogenous fluorescence (Table 3). The light emitted during the fluorescence process is also absorbed and scattered, and is influenced by fibrous anisotropic structures having the properties of imperfect optical fibers. This effect makes it challenging to analyze the distribution pattern on the skin surface and limits the practical application of fluorescent diagnostics. Empirical assessment of signal distortion from an intradermally located light source has become the main focus of this work.

Theoretically, any fluorophore listed in Table 3 could be the object of our study. However, not all of these are equally informative for oncodiagnostics. According to the published data, changes in the characteristic fluorescence of tryptophan [24], collagen [25], NADH [8] and especially

Таблица 3
Спектральные характеристики основных эндогенных флуорофоров кожи

Table 3
Spectral characteristics of the most common endogenous skin fluorophores

Название Name	Длина волны максимального возбуждения λ_{EX}, нм Maximum excitation wavelength λ_{EX}, nm	Длина волны максимального испускания флуоресценции λ_{FL}, нм Maximum fluorescence emission wavelength λ_{FL}, nm
НАД(Ф)Н / NAD(P)H	365	420-490
Кератин / Keratin	355-405	450
Коллаген/Эластин Collagen/Elastin	300-340	390-430
Липофусцин Lipofuscin	400-500	480-700
Пироксидин Pyroxidine	320	390
Порфирины Porphyrins	405	630-700
Тирозин / Tyrosine	220, 275	305
Триптофан Tryptophan	250-290	320-350
Флавины / Flavins	450	520-535

protoporphyrin IX are of value. PpIX fluorescence analysis is widely used in the examination and treatment of patients with malignant neoplasms, as well as in their postoperative care [10, 26-29]. Therefore, we have focused our basic interest on this particular compound.

We have also chosen to focus on the periorbital region, which is known for its uneven topography and high cosmetic and functional requirements.

The choice of a pig as a model for the experiment was not random. Unlike accepted laboratory animals (dogs, cats, rabbits, and mice), the size of its facial skull is comparable to that of humans. Moreover, similarly to humans, a pig does not have much hair in the periorbital region.

In the course of image preprocessing, isolines of the brightness gradient of the red channel were derived. Their shape was later used to assess the correspondence between patterns in which light is dispersed in tissues from an external and an internal source. Note that the "ovality" of the light distribution in the projection onto the skin surface was generally greater than the diffuser's impact in all directions (see Table 1).

In most studies on optics, the authors prefer to use ellipse parameters to describe the correspondence of light distribution [19, 30-32]. This is partly due to the possibility of multiple convolutions of the data, but also because an ellipse is a cross section of the indicatrix of scattering, which is commonly used to describe anisotropy of optical properties. Nevertheless, we assumed that in the conditions we have modeled, approximation of the brightness gradient with an ellipse might destroy critical details of light propagation in tissues, like, for example, thin optical "apophyses" associated with stacks of unidirectional fibers in narrow skin folds, or with a zone of continued tumor growth. Therefore, we have decided not only to evaluate the parameters of the approximating ellipses, but also to perform a quantitative assessment of the correspondence using the correlation method. For that, the *k* coefficient from the linear regression equation, $Y=k*X+b$, that describes point clouds plotted for each pair of brightness isolines, was chosen as the correspondence criterion. The higher the correlation, the closer the *k* value was to 1. Please note that the proposed correlation method will only be accurate if the isolines are clearly elongated in one or more directions, but not largely distorted by noise from minor surface irregularities, such as skin pores.

To sum up, the correlation between the skin projections of light distribution from an internal and an external source in this experiment should be regarded as high in two cases:

1) **both axis ratios of the ellipses corresponding to one pair of isolines are within the range of 0.95 to 1.05** (deviation of less than 5% was considered as insignificant). This means that both light sources produce roughly *circular* spots on the skin surface, which can happen when the light travels through a relatively homogeneous and isotropic medium in both tests;
2) **the axis ratios of the ellipses corresponding to one pair of isolines fall outside the range 0.95 to 1.05, but *k* is greater than 0.7** (i.e. strong or very strong correlation according to the Chaddock scale). This means that both light spots on the skin surface are *non-circular but still similar*, which can happen when the light spreads unevenly in different directions, but the directivity of light distribution correlates with the average strength of the signal between the tests.

In the studied skin areas, the correlation of light distribution from the two sources generally increased with the distance from the origin (Fig. 5A-C and Table 2), except for the zone of interest 4, where the trend was the opposite. Perhaps, the latter was due to a more accurate alignment between the locus of the maximum light density at Test 1 (internal light source) and the position of the external light source at Test 2. Besides uneven light distribution across the given area, another possible explanation for that could be an error in determining the position of the tip of the drill with a magnetic pendulum. Due to the fact that the pig's head was fixed almost vertically (Fig. 1), it is logical to assume that there could be a displacement of the pendulum under the influence of gravity in the moment when the drill and the pendulum were located in the same horizontal plane. An empirical test of this assumption in the air showed that

such a 'slip' may be up to 0.80+/-0.05 mm. At the distance from the light source, however, this effect diminishes and the correspondence increases (Fig. 5).

Also, attention should be drawn to the results obtained in the zone of interest 2, where the *k* coefficient was low for all pairs of isolines and even took a negative value for the pair 1, which is probably due to the presence of multiple "coarse" skin pores that caused scalloped edges of brightness gradients. Nevertheless, the overall isometricity of the gradients remained high.

And finally, since we have selected truly "similar" isolines (not equalized by their mean X and Y values), each of the point clouds in Figure 4 appears to be slightly shifted relative to the X=Y line. We could, of course, use an iterative or analytical method to obtain perfectly matched pairs of isolines in a quasi-smooth gradient field from the very beginning, but this would not be very useful in illustrating the correlation of light distribution in tissues for the two arrangements of light sources.

Having analyzed the described results, we can conclude that the registration of the light distribution pattern from a source applied to the skin surface allowed us to satisfactorily evaluate light propagation from an intradermal source. Quantitative estimations were positive for the outer regions of all zones of interest, except for the zone 2, as well as the inner regions of the zones 1 and 4. The relative failure of the zone 2 tests, as stated above, can be attributed to significant skin irregularities (larger than the selected filtering window) and an obvious artifact produced by the optical fiber within the field of view of the camera.

We suggest that "correction for anisotropy" could be incorporated into the fluorescence diagnostics routine. However, this would require some kind of a device that projects light of a specific wavelength onto the skin surface and which is a) simple enough to enable rapid examination and b) free from geometric distortions caused by opaque structural elements in the field of view of the camera. Having these requirements met, such a device could be used in practical oncology, including ophthalmology, since it is the periorbital neoplasms that are often located at the junctions of tissues with different optical properties.

Conclusion

This experiment has clearly demonstrated the previously theoretical relationship between the fluorescence distribution pattern of a tumor on the one hand, and the condition and/or topography of the tissues containing this tumor, on the other. It has also proved the possibility of using an external light source to assess the local scattering anisotropy of the skin, particularly in the periorbital region.

REFERENCES

1. Kaprin A.D., Starinsky V.V., Shakhzadova A.O. eds. Malignant neoplasms in Russia in 2020 (morbidity and mortality). M.: P.A. Herzen Moscow Oncology Research Institute. – 2021. (In Russ.)
2. Sung H., Ferlay J., Siegel R.L., Laversanne M., Soerjomataram I., Jemal A., Bray F. Global cancer statistics 2020: GLOBOCAN estimates of incidence and mortality worldwide for 36 cancers in 185 countries. *CA Cancer J Clin*, 2021, Vol. 71, pp. 209-249. https://doi.org/10.3322/caac.21660
3. Peris K., Fargnoli M.C., Garbe C., Kaufmann R., Bastholt L., Seguin N.B., Bataille V., Marmol V. D., Dummer R., Harwood C.A., Hauschild A., Höller C., Haedersdal M., Malvehy J., Middleton M.R., Morton C.A., Nagore E., Stratigos A.J., Szeimies R.M., Tagliaferri L., Trakatelli M., Zalaudek I., Eggermont A., Grob J.J. Diagnosis and treatment of basal cell carcinoma: European consensus-based interdisciplinary guidelines. *Eur J Cancer*, 2019, Vol. 118, pp. 10-34.
4. Vornicescu C., Șenilă S.C., Bejinariu N.I., Vesa Ș.C., Boșca A.B., Chirilă D.N., MelincoviciC.S., Soriță O., Mihu C.M. Predictive factors for the recurrence of surgically excised basal cell carcinomas: A retrospective clinical and immunopathological pilot study. *Experimental and Therapeutic Medicine*, 2021, Vol. 22(5), pp.1336. https://doi.org/10.3892/etm.2021.10771
5. Policard A. Etudes sur les aspects offerts par des tumeurs experimentales ex aminées a la lumière de Wood. *C R Soc Biol*, 1924, Vol. 91, pp. 1423-1428.
6. GalkinaE.M., Utz S.R. Fluorescence diagnosis in dermatology (review). *Saratov Journal of Medical Scientific Research*, 2013, Vol. 9(3), pp. 566-572. (In Russ.)
7. Wizenty J., Schumann T., Theil, D., Stockmann M., Pratschke J., Tacke F., Aigner F., Wuensch T. Recent Advances and the Potential for Clinical Use of Autofluorescence Detection of Extra-Ophthalmic Tissues. *Molecules*, 2020, Vol. 25(9), pp. 2095.
8. Croce A.C., Bottiroli G. Autofluorescence spectroscopy and imaging: A tool for biomedical research and diagnosis. *Eur. J. Histochem*, 2014, Vol. 58. – P. 2461.
9. Vo-Dinh T. Biomedical photonics handbook: biomedical diagnostics. *CRC press. Boca Raton*. – 2014.
10. McNicholas K., MacGregor M.N., Gleadle J.M. In order for the light to shine so brightly, the darkness must be present-why do cancers fluoresce with 5-aminolaevulinic acid? *Br J Cancer,* 2019, Vol. 121(8), pp. 631-639. https://doi.org/10.1038/s41416-019-0516-4.
11. Pavlova NN, Thompson CB. The emerging hallmarks of cancer metabolism. *Cell Metab,* 2016, Vol. 23(1), pp. 27-47. https://doi.org/10.1016/j.cmet.2015.12.006.

ЛИТЕРАТУРА

1. Kaprin A.D., Starinsky V.V., Shakhzadova A.O. eds. Malignant neoplasms in Russia in 2020 (morbidity and mortality). M.: P.A. Herzen Moscow Oncology Research Institute. – 2021. (In Russ.)
2. Sung H., Ferlay J., Siegel R.L., Laversanne M., Soerjomataram I., Jemal A., Bray F. Global cancer statistics 2020: GLOBOCAN estimates of incidence and mortality worldwide for 36 cancers in 185 countries // CA Cancer J Clin. – 2021. – Vol.71. – P. 209-249. https://doi.org/10.3322/caac.21660
3. Peris K., Fargnoli M.C., Garbe C., Kaufmann R., Bastholt L., Seguin N.B., Bataille V., Marmol V. D., Dummer R., Harwood C.A., Hauschild A., Höller C., Haedersdal M., Malvehy J., Middleton M.R., Morton C.A., Nagore E., Stratigos A.J., Szeimies R.M., Tagliaferri L., Trakatelli M., Zalaudek I., Eggermont A., Grob J.J. Diagnosis and treatment of basal cell carcinoma: European consensus-based interdisciplinary guidelines // Eur J Cancer. – 2019. – Vol. 118. – P.10-34.
4. Vornicescu C., Șenilă S.C., Bejinariu N.I., VesaȘ.C., Boșca A.B., Chirilă D.N., MelincoviciC.S., Soriță O., Mihu C.M. Predictive factors for the recurrence of surgically excised basal cell carcinomas: A retrospective clinical and immunopathological pilot study // Experimental and Therapeutic Medicine. – 2021. – Vol. 22(5). – P.1336. https://doi.org/10.3892/etm.2021.10771
5. Policard A. Etudes sur les aspects offerts par des tumeurs experimentales ex aminées a la lumière de Wood // C R Soc Biol. – 1924. – Vol. 91. – P. 1423-1428.
6. GalkinaE.M., Utz S.R. Fluorescence diagnosis in dermatology (review) // Saratov Journal of Medical Scientific Research. – 2013. – Vol. 9(3). – P. 566-572. (In Russ.)
7. Wizenty J., Schumann T., Theil, D., Stockmann M., Pratschke J., Tacke F., Aigner F., Wuensch T. Recent Advances and the Potential for Clinical Use of Autofluorescence Detection of Extra-Ophthalmic Tissues // Molecules. – 2020. – Vol. 25(9). – P. 2095.
8. Croce A.C., Bottiroli G. Autofluorescence spectroscopy and imaging: A tool for biomedical research and diagnosis // Eur. J. Histochem. – 2014. – Vol. 58. – P. 2461.
9. Vo-Dinh T. Biomedical photonics handbook: biomedical diagnostics // CRC press. Boca Raton. – 2014.
10. McNicholas K., MacGregor M.N., Gleadle J.M. In order for the light to shine so brightly, the darkness must be present-why do cancers fluoresce with 5-aminolaevulinic acid? // Br J Cancer. – 2019. – Vol. 121(8). – P. 631-639. https://doi.org/10.1038/s41416-019-0516-4.
11. Pavlova N.N., Thompson C.B. The emerging hallmarks of cancer metabolism // Cell Metab. – 2016. – Vol. 23 (1). – P.27-47. https://doi.org/10.1016/j.cmet.2015.12.006.

12. Potapov A.A., Goriaĭnov S.A., Loshchenov V.B., Savel'eva T.A., Gavrilov A.G., Okhlopkov V.A., Zhukov V.Iu., Zelenkov P.V., Gol'bin D.A., Shurkhaĭ V.A., Shishkina L.V., Grachev P.V., Kholodtsova M.N., Kuz'min S.G., Vorozhtsov G.N., Chumakova A.P. Intraoperative combined spectroscopy (optical biopsy) of cerebral gliomas. *ZhVoprNeirokhirIm N. N. Burdenko*, 2013, Vol. 77(2), pp. 3-10. (In Eng., Russ.)
13. Na R., Stender I.M., Wulf H.C. Can autofluorescence demarcate basal cell carcinoma from normal skin? A comparison with protoporphyrin IX fluorescence. *Acta Derm Venereol*, 2001, Vol. 81, pp. 246-249. https://doi.org/10.1080/00015550152572859
14. Hegyi J., Hegyi V., New developments in fluorescence diagnostics. In: Michael R. Hamblin, Pinar Avci, Gaurav K. Gupta, eds. *Imaging in Dermatology. Academic Press*, 2016, pp. 89-94. https://doi.org/10.1016/B978-0-12-802838-4.00009-1
15. Grusha Ia.O., Kiryushchenkova N.P., Novikov I.A., Fedorov A.A., Ismailova D.S. Histological verification of autofluorescence borders of periorbital skin tumors. *Vestnik Oftalmologii*, 2020, Vol. 136(6), pp. 32-41. (In Russ.) https://doi.org/10.17116/oftalma202013606132
16. Kienle A., Foschum F., Hohmann A. Light propagation in structural anisotropic media in the steady-state and time domains. *Phys. Med. Biol*, 2013, Vol. 58(17), pp. 6205. https://doi.org/10.1088/0031-9155/58/17/6205
17. Jacques S.L. Optical properties of biological tissues: a review. *Phys Med Biol*, 2013, Vol. 58(11), pp. 37-61. https://doi.org/0.1088/0031-9155/58/11/R37.
18. Nickell S. et al. Anisotropy of light propagation in human skin. *Phys. Med. Biol,* 2000, Vol. 45, pp. 2873-2886.
19. Tuchin V.V. Lasers and optical fibers in biomedical studies (2d ed.). *Fizmatlit*, 2010 (In Russ.)
20. Tuchin V.V. Optical biomedical diagnosis. *Izvestiya of Saratov University. Physics*, 2005, Vol. 1(5), pp. 39-53. (In Russ.) https://doi.org/10.18500/1817-3020-2005-5-1-39-53.
21. Anderson RR, Parrish JA. The optics of human skin. *J Invest Dermatol*, 1981, Vol. 77 (1), pp. 13-9. https://doi.org/10.1111/1523-1747.ep12479191.
22. Colas V., Daul C., Khairallah G., Amouroux M., Blondel W. Spatially resolved diffuse reflectance and autofluorescence photon depth distribution in human skin spectroscopy: a modeling study. *Proc. SPIE* 11553, *Optics in Health Care and Biomedical Optics X*, 115531A. https://doi.org/10.1117/12.2575069
23. Brancaleon L., Durkin A.J., Tu J.H., Menaker G., Fallon J.D., Kollias N. In vivo Fluorescence Spectroscopy of Nonmelanoma Skin Cancer. *Photochemistry and Photobiology*, 2001, Vol. 73(2), pp. 178-183. https://doi.org/10.1562/0031-8655(2001)073
24. Masuda Y., Ogura Y., Inagaki Y., Yasui T., Aizu Y. Analysis of the influence of collagen fibres in the dermis on skin optical reflectance by Monte Carlo simulation in a nine-layered skin model. *Skin Res Technol*, 2018, Vol. 24, pp. 248-255. https://doi.org/10.1111/srt.12421
25. Smirnova O.D., Rogatkin D., Litvinova K. Collagen as in vivo quantitative fluorescent biomarkers of abnormal tissue changes. *J. Innov. Opt. Health Sci*, 2012, Vol. 05(2), pp.1250010.
26. Yagi R., Kawabata S., Ikeda N. et al. Intraoperative 5-aminolevulinic acid-induced photodynamic diagnosis of metastatic brain tumors with histopathological analysis. *World J SurgOnc,* 2017, Vol. 15, pp.179. https://doi.org/10.1186/s12957-017-1239-8
27. Redondo P., Marquina M., Pretel M., Aguado L., Iglesias M.E. Methyl-ALA-Induced Fluorescence in Photodynamic Diagnosis of Basal Cell Carcinoma Prior to Mohs Micrographic Surgery. *ArchDermatol*, 2008, Vol. 144(1), pp.115-117. https://doi.org/10.1001/archdermatol.2007.3
28. Kiryushchenkova N.P., Grusha Y., The use of autofluorescence diagnostics in monitoring and evaluating the effectiveness of local chemotherapy for superficial basal cell carcinoma of the skin (clinical case). *Modern technologies in ophthalmology*, 2020, Vol. 4 (35), pp.162-163. (In Russ.) https://doi.org/10.25276/2312-4911-2020-4-162-163
29. Hefti M., von Campe G., Moschopulosa M., Siegnerb A., Looserc H., Landolt H. 5-aminolaevulinic acid-induced protoporphyrin IX fluorescence in high-grade glioma surgery. *SWISS MED WKLY*, 2008, Vol. 138(11-12), pp.180-185.
30. Sapronov M.V., Skornyakova N.M. Computer visualization of Rayleigh scattering indicatrix in dynamic. *Scientific visualization*, 2017, Vol.3(9), pp.42-53. (In Russ.)
31. Kalyagina N., Loschenov V., Wolf D., Daul C., Blondel W., Savelieva T. Experimental and Monte Carlo investigation of visible diffuse-reflectance imaging sensitivity to diffusing particle size changes in an optical model of a bladder wall. *Applied Physics B*, 2011, Vol. 105. (3), pp. 631-639. doi:10.1007/s00340-011-4678-x
32. Colas V., Amouroux M., Daul C., Perrin-Mozet C., Blondel W. Comparative study of optical properties estimation on liquid optical phantoms using spatially-resolved diffuse reflectance spectroscopy and double integrating spheres methods. *Proc. SPIE 12147. – Tissue Optics and Photonics II*, pp. 1214705. https://doi.org/10.1117/12.2621496

12. Potapov A.A., Goriaĭnov S.A., Loshchenov V.B., Savel'eva T.A., Gavrilov A.G., Okhlopkov V.A., Zhukov V.Iu., Zelenkov P.V., Gol'bin D.A., Shurkhaĭ V.A., Shishkina L.V., Grachev P.V., Kholodtsova M.N., Kuz'min S.G., Vorozhtsov G.N., Chumakova A.P. Intraoperative combined spectroscopy (optical biopsy) of cerebral gliomas // ZhVoprNeirokhirIm N. N. Burdenko. – 2013. – Vol. 77(2). – P. 3-10. (In Eng., Russ.)
13. Na R., Stender I.M., Wulf H.C. Can autofluorescence demarcate basal cell carcinoma from normal skin? A comparison with protoporphyrin IX fluorescence // Acta Derm Venereol. – 2001. – Vol. 81. – P. 246-249. https://doi.org/10.1080/00015550152572859
14. Hegyi J., Hegyi V., New developments in fluorescence diagnostics. In: Michael R. Hamblin, Pinar Avci, Gaurav K. Gupta, eds // Imaging in Dermatology. Academic Press. – 2016. – P. 89-94. https://doi.org/10.1016/B978-0-12-802838-4.00009-1
15. Grusha Ia.O., Kiryushchenkova N.P., Novikov I.A., Fedorov A.A., Ismailova D.S. Histological verification of autofluorescence borders of periorbital skin tumors // Vestnik Oftalmologii. – 2020. – Vol. 136(6). – P. 32-41. (In Russ.) https://doi.org/10.17116/oftalma202013606132
16. Kienle A., Foschum F., Hohmann A. Light propagation in structural anisotropic media in the steady-state and time domains // Phys. Med. Biol. – 2013. – Vol. 58(17). – P. 6205. https://doi.org/10.1088/0031-9155/58/17/6205
17. Jacques S.L. Optical properties of biological tissues: a review // Phys Med Biol. – 2013. – Vol. 58(11). – P. 37-61. https://doi.org/0.1088/0031-9155/58/11/R37.
18. Nickell S. et al. Anisotropy of light propagation in human skin // Phys. Med. Biol. – 2000. – Vol. 45. – P. 2873-2886.
19. Tuchin V.V. Lasers and optical fibers in biomedical studies (2d ed.) // Fizmatlit. – 2010 (In Russ.)
20. Tuchin V.V. Optical biomedical diagnosis // Izvestiya of Saratov University. Physics. – 2005. – Vol. 1(5). – P. 39-53. (In Russ.) https://doi.org/10.18500/1817-3020-2005-5-1-39-53.
21. Anderson RR, Parrish JA. The optics of human skin // J Invest Dermatol. – 1981. – Vol.77 (1). – P. 13-9. https://doi.org/10.1111/1523-1747.ep12479191.
22. Colas V., Daul C., Khairallah G., Amouroux M., Blondel W. Spatially resolved diffuse reflectance and autofluorescence photon depth distribution in human skin spectroscopy: a modeling study // Proc. SPIE 11553.- Optics in Health Care and Biomedical Optics X. – 115531A. https://doi.org/10.1117/12.2575069
23. Brancaleon L., Durkin A.J., Tu J.H., Menaker G., Fallon J.D., Kollias N. *In vivo* Fluorescence Spectroscopy of Nonmelanoma Skin Cancer // Photochemistry and Photobiology. –2001. – Vol. 73(2). – P. 178-183. https://doi.org/10.1562/0031-8655(2001)073<0178: IVFSON>2.0.CO;2
24. Masuda Y., Ogura Y., Inagaki Y., Yasui T., Aizu Y. Analysis of the influence of collagen fibres in the dermis on skin optical reflectance by Monte Carlo simulation in a nine-layered skin model // Skin Res Technol. – 2018. – Vol. 24. – P. 248-255. https://doi.org/10.1111/srt.12421
25. Smirnova O.D., Rogatkin D., Litvinova K. Collagen as in vivo quantitative fluorescent biomarkers of abnormal tissue changes // J. Innov. Opt. Health Sci. – 2012. – Vol. 05(2). – P.1250010.
26. Yagi R., Kawabata S., Ikeda N. *et al.* Intraoperative 5-aminolevulinic acid-induced photodynamic diagnosis of metastatic brain tumors with histopathological analysis // World J SurgOnc – 2017. – Vol. 15 – P. 179. https://doi.org/10.1186/s12957-017-1239-8
27. Redondo P., Marquina M., Pretel M., Aguado L., Iglesias M.E. Methyl-ALA-Induced Fluorescence in Photodynamic Diagnosis of Basal Cell Carcinoma Prior to Mohs Micrographic Surgery // ArchDermatol. – 2008. – Vol. 144(1). – P. 115-117. https://doi.org/10.1001/archdermatol.2007.3
28. Kiryushchenkova N.P., Grusha Y., The use of autofluorescence diagnostics in monitoring and evaluating the effectiveness of local chemotherapy for superficial basal cell carcinoma of the skin (clinical case) // Modern technologies in ophthalmology. – 2020. – Vol. 4 (35). – P. 162-163. (In Russ.) https://doi.org/10.25276/2312-4911-2020-4-162-163
29. Hefti M., von Campe G., Moschopulosa M., Siegnerb A., Looserc H., Landolt H. 5-aminolaevulinic acid-induced protoporphyrin IX fluorescence in high-grade glioma surgery // SWISS MED WKLY – 2008. –Vol. 138(11-12). – P. 180-185.
30. Sapronov M.V., Skornyakova N.M. Computer visualization of Rayleigh scattering indicatrix in dynamic // Scientific visualization. – 2017. – Vol. 3(9). – P. 42-53. (In Russ.)
31. Kalyagina N., Loschenov V., Wolf D., Daul C., Blondel W., Savelieva T. Experimental and Monte Carlo investigation of visible diffuse-reflectance imaging sensitivity to diffusing particle size changes in an optical model of a bladder wall // Applied Physics B. – 2011. – Vol. 105(3). – P. 631-639.doi:10.1007/s00340-011-4678-x
32. Colas V., Amouroux M., Daul C., Perrin-Mozet C., Blondel W. Comparative study of optical properties estimation on liquid optical phantoms using spatially-resolved diffuse reflectance spectroscopy and double integrating spheres methods // Proc. SPIE 12147. – Tissue Optics and Photonics II. – P. 1214705. https://doi.org/10.1117/12.2621496